### Rise and fall of patterns in driven-dissipative Rydberg polaritons

Hadiseh Alaeian 1,2,\* and Valentin Walther 3,2,†

<sup>1</sup>Elmore Family School of Electrical and Computer Engineering, Purdue University, West Lafayette, Indiana 47906, USA

<sup>2</sup>Department of Physics and Astronomy, Purdue University, West Lafayette, Indiana 47906, USA

<sup>3</sup>Department of Chemistry, Purdue University, West Lafayette, Indiana 47906, USA

(Received 24 October 2023; revised 29 March 2024; accepted 24 June 2024; published 15 July 2024)

In this study, we present an exploration of spontaneous symmetry breaking and pattern formation in the driven-dissipative system of Rydberg exciton polaritons with long-range interactions. Our investigation unravels the pattern formations through modulational instability, characterized by scales in the micron range. We observe the dynamics of the polariton ensemble, studying the emergence of metastable patterns and their eventual collapse in the long-time limit. This phenomenon is attributed to the destructive interference between the polariton state and the external drive within the ensemble. Further, we delineate conditions conducive to the stable formation of patterns under incoherent pumping. These findings open up various avenues for delving into the burgeoning realm of driven-dissipative and long-range interacting gases through the unique characteristics of Rydberg excitons.

DOI: 10.1103/PhysRevResearch.6.033065

#### I. INTRODUCTION

Spontaneous pattern formation is a widespread phenomenon across various disciplines, ranging from cosmology [1] to biology [2] and condensed matter physics [3]. While there is no universal microscopic mechanism giving rise to stationary patterns in these diverse systems, they all share a complex interplay of dispersion, interactions of various length scales, and external driving forces.

In quantum systems, cold atoms have evolved into a potent tool for simulating a diverse range of phenomena in *closed* quantum systems, encompassing spontaneous symmetry breaking and the formation of patterns. Numerous theoretical and experimental investigations have unveiled various phases and the emergence of patterns in long-range interacting and dipolar Bose-Einstein condensates (BECs) [4–12]. Additionally, studies have explored roton instabilities in quasi-one-dimensional (quasi-1D) dipolar BECs subjected to a periodic lattice potential [13], hexagonal pattern formations in Rydberg BECs [14–17], and the prediction of quasicrystalline structures in optical feedback systems [15,18].

Concurrently, exciton polaritons, characterized as hybrid light-matter quasiparticles with optical nonlinearities, have surfaced as an alternative avenue for quantum simulation. Unlike cold atoms, polaritons are *open* quantum systems

\*Contact author: halaeian@purdue.edu †Contact author: vwalther@purdue.edu

Published by the American Physical Society under the terms of the Creative Commons Attribution 4.0 International license. Further distribution of this work must maintain attribution to the author(s) and the published article's title, journal citation, and DOI.

and exhibit driven-dissipative dynamics which constitute a focal point in ongoing research [19–21]. Leveraging their adaptable potential landscape and tunable interaction features, polaritons present a versatile platform for the exploration of *driven-dissipative* phenomena [22–24]. Moreover, the direct access to their photonic component facilitates the investigation of states' quantum statistical properties. So far, the majority of the explored phenomena in exciton polaritons have revolved around short-range interactions [22]. The observation of highly excited Rydberg states of excitons in Cu<sub>2</sub>O [25,26] and the recent demonstration of Rydberg exciton polaritons [27–29] in planar cavities introduce the opportunity to explore the largely uncharted territory of systems combining long-range interactions, drive, and dissipation.

In this work, we investigate whether the characteristic pattern formation fueled by long-range interactions, typically observable in cold dipolar atomic gases, can be achieved in Rydberg polaritons. We delve into the dynamic evolution of polariton phases where the homogeneous state becomes unstable, leading to finite-range instability behavior and pattern formation during the system's evolution. Additionally, we scrutinize the long-term stability of this patterned phase in an open system compared to a closed one, as depicted in Figs. 1(c) and 1(d). Our calculations indicate that unlike in closed systems, the stability of the driven-dissipative case is contingent on the type of external pump. Given the high tunability of Rydberg polaritons through parameters such as the principal quantum number, cavity parameters, and driving in conjunction with their distinctive long-range interactions, Rydberg polaritons make a unique platform for investigating driven-dissipative quantum many-body phenomena.

We consider an unconfined polariton formed by a 2D cavity encapsulating a layer hosting Rydberg excitons, as depicted in Fig. 1(a). With the cavity field treated at the mean-field level, the excitons and their correlations can be solved exactly and

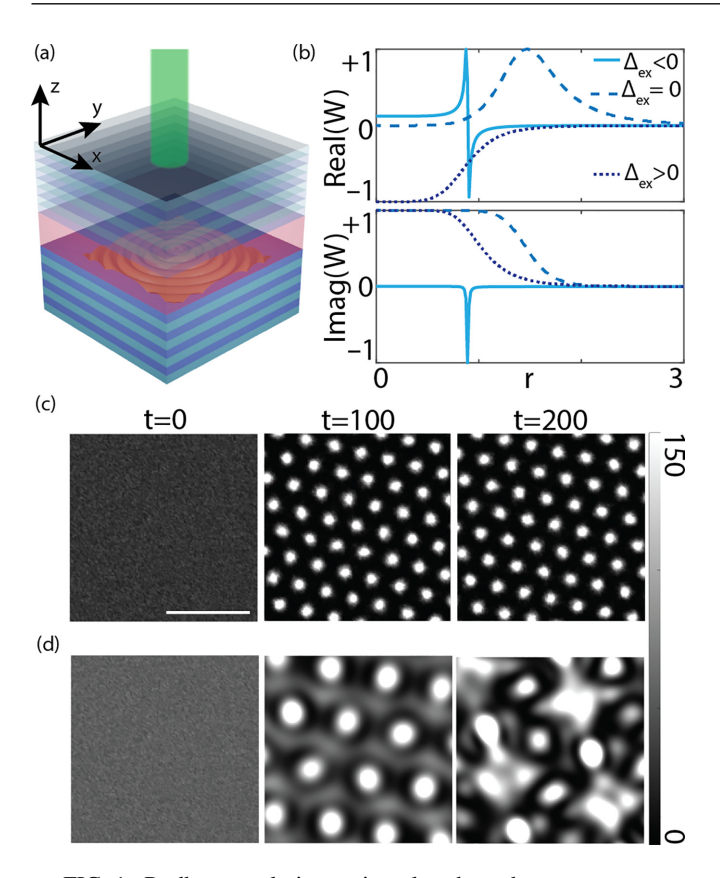


FIG. 1. Rydberg polaritons in closed and open systems. (a) Schematics of a 2D optical cavity encapsulating the Rydberg excitonic material. (b) Normalized nonlinear W(r) as a function of r showing the tunability of dispersive (top) and dissipative (bottom) effective soft-core potential via the exciton detuning,  $\Delta_{ex}$ . Snapshots of cavity-field intensity in (c) a closed system with  $g = 1, C_6 =$ -1,  $\Delta = -1$  and (d) a coherently driven open system with  $\Delta_{ex} =$ 6,  $\gamma = 0.1$ ,  $\kappa = 0.5$ ,  $C_6 = -1$ ,  $\Delta_c = 2$ , highlighting the pattern formations in both cases while contrasting their stability. The white scale bar corresponds to L = 10. Initial field at t = 0 is homogeneous with  $|E_0|^2 = 10$  and  $|E_0|^2 = 25$ , respectively, and subject to random noise.

analytically to the third order in terms of the field, which leads to the following generalized Gross-Pitaevskii equation (GPE) describing the cavity-field dynamics only as (see Appendix A for details on the GPE derivation)

$$i\partial_{t}\mathcal{E}(\mathbf{r},t) = \left[ -\frac{\hbar}{2m_{\rm ph}} \nabla^{2} + i\chi^{(1)} - i\frac{\Gamma_{c}}{2} + \int d\mathbf{r}' W(\mathbf{r} - \mathbf{r}') |\mathcal{E}(\mathbf{r}',t)|^{2} \right] \mathcal{E}(\mathbf{r},t) + \text{drive.}$$
(1)

$$\mathcal{B} = \begin{pmatrix} \frac{\mathbf{k}^2}{2} + i\left(\chi^{(1)} - \frac{\Gamma_c}{2}\right) + 2\pi |E_0|^2 [\tilde{W}(\mathbf{k}) + \tilde{W}(0)] \\ -2\pi E_0^{*2} \tilde{W}^*(\mathbf{k}) \end{pmatrix}$$

where  $\tilde{W}(\mathbf{k})$  is the Fourier transform of  $W(\mathbf{r})$ .

In this equation,  $\chi^{(1)}$  and W are the effective linear and nonlinear optical susceptibility, respectively, mediated by the exciton-exciton interaction with the following explicit forms:

$$\chi^{(1)} = -\frac{2g^2}{\Gamma_{\text{ex}}},\tag{2}$$

$$\chi^{(1)} = -\frac{2g^2}{\Gamma_{\text{ex}}},$$

$$W(\mathbf{r}) = -\frac{16g^4}{|\Gamma_{\text{ex}}|^2 \Gamma_{\text{ex}}} \frac{U(\mathbf{r})}{\Gamma_{\text{ex}} + iU(\mathbf{r})},$$
(3)

where g is the vacuum Rabi coupling between the excitons and cavity mode and  $U(\mathbf{r})$  is the pairwise long-range van der Waals interaction between excitons as  $U(\mathbf{r}) = \frac{C_6}{|\mathbf{r} - \mathbf{r}'|^6}$  [30]. The complex-valued exciton and cavity decay rates  $\Gamma_{\rm ex}$  and  $\Gamma_c$ are related to the cavity  $\Delta_c$  and exciton detuning  $\Delta_{ex}$  as well as the decay rates of the Rydberg state  $\gamma$  and cavity photons  $\kappa$ , via

$$\Delta_c = \omega_p - \omega_c, \quad \Gamma_c = \kappa - 2i\Delta_c,$$
 (4)

$$\Delta_{\rm ex} = \omega_p - \omega_{\rm ex}, \quad \Gamma_{\rm ex} = \gamma - 2i\Delta_{\rm ex}.$$
 (5)

The nonlocal character of the nonlinear susceptibility stems from the long-range interactions between excitons, a potential that depends on the principal quantum number through an n-dependent  $C_6$  coefficient and realizes a dissipative and dispersive soft-core potential, as depicted in Fig. 1(b) [21]. In the rest of the text, we work with the dimensionless quantities

$$\tilde{\mathcal{E}}(\mathbf{r},t) = r_0 \mathcal{E}\left(\frac{\mathbf{r}}{r_0}, \frac{t}{\tau}\right),\tag{6}$$

where c is the speed of light,  $r_0 = L/(n\pi)$  is the effective cavity length, n is the effective refractive index of the excitonic material, and  $\tau = r_0/c$  is the photon travel time within the cavity. These choices of the length scale and timescale help to underline the general features of the system, but we use parameters from experiments on cuprous oxide for all figures and discuss the parameter choices towards the end of this paper (see Appendix E for further information).

#### II. RESULTS

Commonly, excitations can be created either via a coherent pump of the cavity field or an incoherent one, typically describing the excitation via a reservoir [22]. Coherent pumping directly injects photons into the cavity mode and can be described via a driving term as  $iE_0$  in Eq. (1). The dynamics of a fluctuation  $\delta \mathbf{E}(\mathbf{k}, t)$  around any stationary point is then given

$$i\frac{d}{dt} \begin{pmatrix} \delta \mathbf{E}(\mathbf{k}, t) \\ \delta \mathbf{E}^*(-\mathbf{k}, t) \end{pmatrix} = \mathcal{B} \begin{pmatrix} \delta \mathbf{E}(\mathbf{k}, t) \\ \delta \mathbf{E}^*(-\mathbf{k}, t) \end{pmatrix}, \tag{7}$$

where the Bogoliubov matrix  $\mathcal{B}$  for a uniform solution  $E_0$ reads

$$\mathcal{B} = \begin{pmatrix} \frac{\mathbf{k}^2}{2} + i\left(\chi^{(1)} - \frac{\Gamma_c}{2}\right) + 2\pi |E_0|^2 [\tilde{W}(\mathbf{k}) + \tilde{W}(0)] & 2\pi E_0^2 \tilde{W}(\mathbf{k}) \\ -2\pi E_0^{*2} \tilde{W}^*(\mathbf{k}) & -\frac{\mathbf{k}^2}{2} + i\left(\chi^{(1)^*} - \frac{\Gamma_c^*}{2}\right) - 2\pi |E_0|^2 [\tilde{W}^*(\mathbf{k}) + \tilde{W}^*(0)] \end{pmatrix}, \tag{8}$$

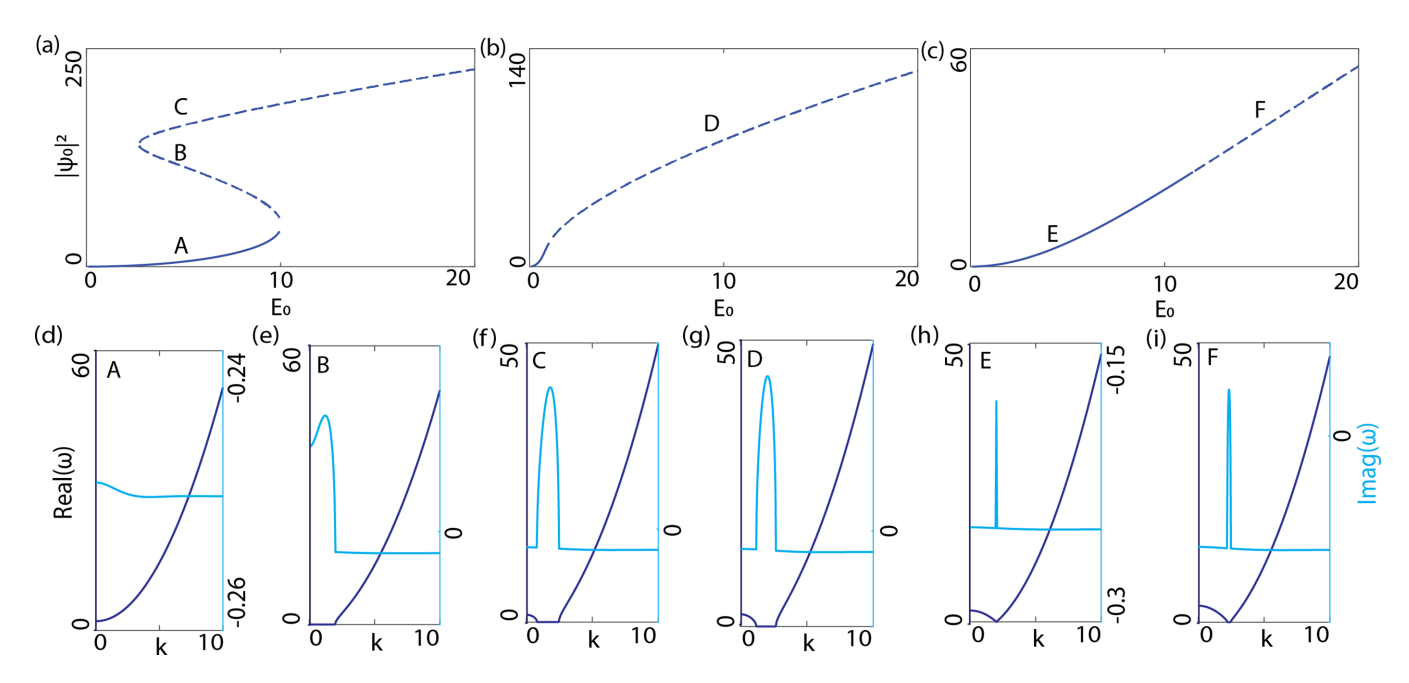


FIG. 2. Homogeneous steady states with coherent drive and the Bogoliubov dispersion. Steady-state photon density  $(|E_0|^2)$  of a Rydberg polariton ensemble, driven by a coherent laser of amplitude  $E_0$  where  $\Delta_{\rm ex}=6$ ,  $\gamma=0.1$ ,  $\kappa=0.5$ ,  $C_6=-1$ , at various cavity detunings (a)  $\Delta_c=-2$ , (b)  $\Delta_c=0$ , and (c)  $\Delta_c=2$ . Stable branches are shown as solid lines in each panel, while the dashed lines show unstable solutions. (d)–(i) The Bogoliubov dispersion of elementary excitations at points (A)–(F) clarifying the (in)stability of each point. In each panel, the dark- (light)-blue line shows the real (imaginary) part of  $\omega(k)$ .

This leads to a dispersion of small fluctuations as

$$\omega_{\pm}(k) = i \left\{ 2\pi |E_0|^2 [\tilde{W}_I(k) + \tilde{W}_I(0)] + \chi_R^{(1)} - \frac{\kappa}{2} \right\}$$

$$\pm \sqrt{\left\{ \frac{k^2}{2} + 2\pi |E_0|^2 [\tilde{W}_R(k) + \tilde{W}_R(0)] - \chi_I^{(1)} - \Delta_c \right\}^2 - 4\pi^2 |E_0|^4 [\tilde{W}_R^2(k) + \tilde{W}_I^2(k)]}, \tag{9}$$

which signifies a modulational instability (MI) where  $\text{Im}[\omega(k)] \geqslant 0$  [31].

Figures 2(a)–2(c) exemplifies the behavior of uniform field intensity ( $|E_0|^2$ ) as a function of the coherent pump strength for cavity detunings  $\Delta_c$  ranging from negative [Fig. 2(a)], to zero [Fig. 2(b)], to positive [Fig. 2(c)]. The homogeneous steady states naturally only depend on the spatial integral over the interaction and are therefore formally equivalent to a system with short-range interactions. Interestingly, the Bogoliubov spectra also show qualitatively very similar features compared to polaritons with contact interactions (cf. [22]): For both types of interactions, a wide array of behaviors can be obtained, including dynamical (in)stability depicted as (dashed) solid lines. For an attractive interaction ( $C_6 \leq 0$ ) as considered here and at negative cavity detuning [Fig. 2(a)], optical multistability emerges. While the middle branch, characterized by the negative slope, is always unstable (dotted line), the two other branches' stabilities depend on the cavity detuning. When both the lower and upper branches are stable and the middle one is unstable, the cavity field follows a hysteretic behavior, i.e., by increasing the pump intensity, eventually, the lower branch mode abruptly jumps into the upper one when the lower branch ends. On the other hand, if the pump intensity is decreased, the field intensity decreases and jumps back down to the lower branch around this dynamically unstable region when the upper branch ends, similar to the response of a polariton ensemble with contact interaction [22].

For a resonant excitation depicted in Fig. 2(b), only one branch exists, typically referred to as the *pump-only* branch, whose stability depends on the pump intensity. As the photon density increases, the nonlinearity modifies the behavior and deviates from the quadratic trend. Since the cavity becomes increasingly detuned with growing photon number, the effective pumping rate decreases, which leads to a sublinear growth of the cavity-field intensity.

For positive cavity detuning as shown in Fig. 2(c), there is only one branch, just as in the resonant case. However, unlike Fig. 2(b), the cavity photon density grows monotonically with the pump intensity due to the small photon number. The attractive potential detunes the cavity further as the photon density increases, and hence the collective nonlinearity remains low, leading to a monotonic growth, almost quadratically.

In Figs. 2(d)-2(i), we present the real (dark blue) and imaginary (light blue) parts of the Bogoliubov dispersion of points (A)–(F) denoted in Figs. 2(a)-2(c), respectively. While the

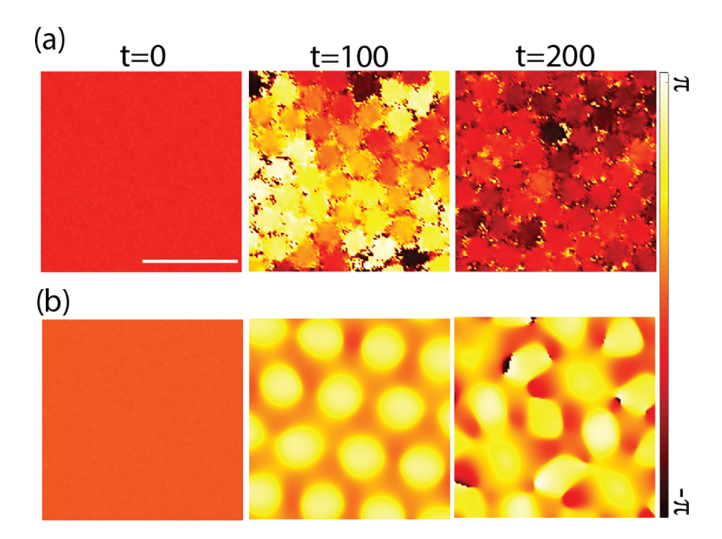


FIG. 3. Phase distribution and polariton flow in closed and open systems. Snapshots of cavity-field phase for (a) closed polariton condensates and (b) the driven-dissipative Rydberg polariton ensemble under a coherent pump, illustrating the stability of the closed case and the ultimate disappearance of the patterns in the open system. The scale bar corresponds to L=10.

stability of the lower branch at point A can be deduced from the always-negative imaginary part in Fig. 2(d), the instability of the middle branch at point B can be deduced from the positive imaginary parts of the dispersion at k = 0 in Fig. 2(e).

At point C on the upper branch, depicted in Fig. 2(f), the two Bogoliubov branches cross in a finite momenta range away from k=0 and give rise to a flat region, i.e.,  $\text{Re}(\omega_{\pm})=0$ . On the other hand, the imaginary parts split and, in the positive-valued regions, the system becomes dynamically unstable. Similar behavior can be observed under resonant excitation, hosting a finite region of MI [cf. Fig. 2(g)]. At larger detunings  $\Delta_c=2$ , the dispersion shows a roton minimum which transitions from stable behavior at weaker pump strengths [Fig. 2(h)] to a finite region of instability, or roton minimum softening, at stronger pump strengths [Fig. 2(i)]. It is worth reiterating that for the homogeneous solution considered above, the instabilities are largely driven by the cavity detuning and parametric scattering, and the long-range nature of the interactions only contributes to smaller corrections.

Therefore, to examine the ensemble's behavior in the presence of the MI, we must time evolve the field dynamics given by the generalized GPE in Eq. (1). Figure 1(d) shows a few snapshots of the cavity-field intensity at point F in Fig. 2(c). Upon starting from a noisy initial state at t=0, extended density patterns are established at longer times, e.g., t = 100. This is in stark contrast to systems with short-range interactions and is, in fact, similar to the closed polariton dynamics depicted in Fig. 1(c). Contrary to the closed system with stable patterns (see Appendix B), however, the patterns in the driven-dissipative polariton cloud are not stable at longer times, as depicted in the field snapshot at t = 200. To shed light on the pattern instability of the open system, we compare the phase distribution of the ensemble in Fig. 3. As can be seen in Fig. 3(a) for the closed case, the polariton cloud establishes a constant phase at equilibrium, corresponding to a uniform chemical potential and hence a vanishing flow of particles. The polariton's phase under drive and dissipation, on the other hand, is not uniform, as depicted in Fig. 3(b). Interference between the inherent phase of the symmetry-broken field and the phase of the external coherent pump leads to a nonvanishing flow towards the high-density points, which limits the lifetime of the patterns [cf. Fig. 3(b), the snapshot at t = 200].

Since the collapse is intimately connected with destructive interference between the cavity photons and the pump laser, we investigate the dynamics of the Rydberg polariton cloud subject to an incoherent drive. The driving term in the generalized nonlocal GPE of Eq. (1) for an incoherent pump intensity  $P(\mathbf{r})$ , with phenomenological coupling and saturation parameters of  $\gamma_R$  and R, can be described as [22,32]

$$i\frac{RP(\mathbf{r})}{2\gamma_R + 2R|\mathcal{E}(\mathbf{r},t)|^2}\tilde{\mathcal{E}}(\mathbf{r},t). \tag{10}$$

Unlike in the coherently driven case, this equation is U(1) symmetric, implying phase freedom of the polariton ensemble. Following a similar approach as for the coherent pump, the fluctuation spectrum around the flat-top solution  $E_0$  can be determined as

$$\omega_{\pm}(\mathbf{k}) = -i \frac{\Gamma_{\text{eff}}(\mathbf{k})}{2} \pm \sqrt{\frac{k^2}{2} \left[ \frac{k^2}{2} + 4\pi E_0^2 \tilde{W}_R(\mathbf{k}) \right] - \frac{\Gamma_{\text{eff}}(\mathbf{k})^2}{4}},$$

where the effective gain/loss rate is defined as

$$\Gamma_{\text{eff}}(\mathbf{k}) = \left[ \frac{R^2 P_0}{(\gamma_R + R|E_0|^2)^2} - 4\pi \tilde{W}_I(\mathbf{k}) \right] E_0^2. \tag{11}$$

Aside from  $\Gamma_{eff}$ , this dispersion is very similar to the closed case; as detailed in Eq. (B4) of Appendix B, similarities in density patterns and their stability are also expected.

Figures 4(a) and 4(b) exemplify the real and imaginary parts of the Bogoliubov dispersion of an incoherently driven cavity, respectively. The dispersion features a finite range of exceptional-point momenta where the real parts of two branches coalesce and their imaginary parts depart from each other. Furthermore, as can be seen in Fig. 4(b), there is a finite range of modulational instability where  $\text{Im}[\omega(k)] \geqslant 0$ . To investigate the emergence of patterns due to MI and their stability, we time evolve the GPE in Eq. (1) with an incoherent pump. The cavity-field intensity and its corresponding phase at a few different times are depicted in Figs. 4(c) and 4(d), respectively. As can be seen, unlike the coherent case, there is no particular phase pattern, and hence no flow of polaritons which would lead to pattern collapse, as highlighted in the field density profile at long times in Fig. 4(c).

### III. CONCLUSION

In this work, we present a study of dynamically unstable phases and pattern formations in Rydberg exciton polaritons featuring long-range interactions in the presence of drive and dissipation. We examined various steady-state phases, encompassing scenarios of multistability and modulational instability. Furthermore, we elucidated the emergence of patterned phases and showed that such patterns can form, but then collapse again under coherent optical pumping. It is important to highlight that the spectral characteristics of

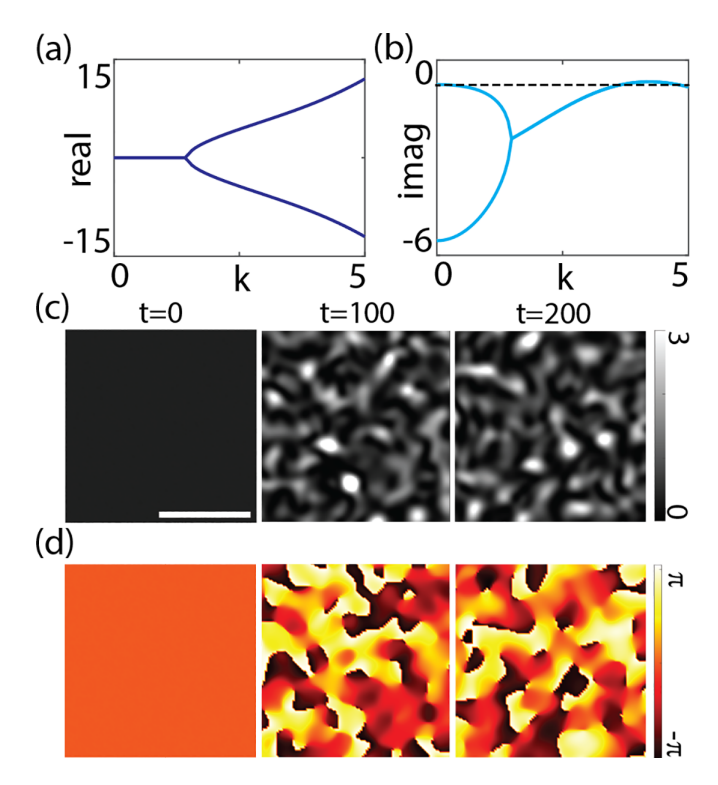


FIG. 4. Dispersion and pattern formation under an incoherent pump. (a) Real and (b) imaginary parts of the Bogoliubov dispersion in an unstable flat-top solution with  $\Delta_{\rm ex}=1$ ,  $\gamma=0.1$ ,  $\kappa=0.5$ ,  $C_6=-1$ . Snapshots of (c) spatial photon density  $|E_0|^2$  and (d) its corresponding phase at various times. The scale bar corresponds to L=10.

the incoherently driven ensemble closely resemble those of the closed system, suggesting a stable long-term behavior. Based on the achievable interaction with Rydberg excitons in cuprous oxide and taking into account their decoherence at n=10, the parameters used in all the figures can be obtained in a cavity with  $L\approx 300$  nm with a moderate finesse of  $\mathcal{F}\approx 20$ , both within reach of experimental capabilities (see Appendix E for a detailed discussion about the cavity and exciton parameters).

As a novel platform, Rydberg polaritons offer a distinctive opportunity to study the physics of strongly interacting open quantum systems. This includes, but is not limited to, the study of quantum fluids supporting solitons and vortices [33,34], Bose-Hubbard models, quantum synchronization in the presence of long-range interactions [35], as well as the emergence of topological effects [36–38], and Faraday patterns [39]. Furthermore, it would be interesting to investigate emerging photonic correlations, as could captured by a beyond-mean-field description [12].

#### **ACKNOWLEDGMENTS**

The authors would like to thank Thomas Pohl and Jens Hertkorn for their insightful discussions, and Furqan Hashmi for his contributions at the early stage of this project. H.A. acknowledges the Purdue University Startup fund and Purdue College of Science, the financial support from the Industry-University Cooperative Research Center Program at the US

National Science Foundation under Grant No. 2224960, and the Air Force Office of Scientific Research under Award No. FA9550-23-1-0489.

#### APPENDIX A: CAVITY-FIELD HAMILTONIAN

Our considered system is driven dissipative since exciton polaritons have a finite lifetime. An accurate description of this driven-dissipative system is given by the quantum master equation. Following the description in [22] for exciton polaritons in a 2D cavity and within the validity range of the rotating wave approximation, the closed-system dynamics of cavity-field-exciton interaction reads

$$\begin{split} \hat{H} &= \int d\mathbf{r} [\hat{\mathcal{E}}^{\dagger}(\mathbf{r}) H_{\text{ph}} \hat{\mathcal{E}}(\mathbf{r}) + \hat{X}^{\dagger}(\mathbf{r}) H_{\text{ex}} \hat{X}(\mathbf{r})] \\ &+ \hbar g \int d\mathbf{r} [\hat{\mathcal{E}}^{\dagger}(\mathbf{r}) \hat{X}(\mathbf{r}) + \text{H.c.}] \\ &+ \frac{1}{2} \iint d\mathbf{r} d\mathbf{r}' \hat{X}^{\dagger}(\mathbf{r}) \hat{X}^{\dagger}(\mathbf{r}') V(|\mathbf{r} - \mathbf{r}'|) \hat{X}(\mathbf{r}') \hat{X}(\mathbf{r}) \\ &+ \text{drive,} \end{split}$$

where  $\hat{\mathcal{E}}^{\dagger}(\mathbf{r})$ ,  $\hat{X}^{\dagger}(\mathbf{r})$  are the cavity and exciton creation field operators at position  $\mathbf{r}$ , respectively, and V is the general nonlocal interaction between two excitons. Because of the finite lifetime of polaritons, the cavity has to be continuously replenished, i.e., driven here, and its steady state results from a dynamical balance between pumping and loss.

To find an effective Hamiltonian description for the photon field inside the cavity  $\mathcal{E}(\mathbf{r})$ , we start from the approximated dispersion of the photons as  $E_{\rm ph}=\hbar\omega=\hbar ck/n$ , where n is the refractive index of the material filling the cavity and k is the photon momentum. Expressing the momentum in terms of the in-plane and perpendicular to the cavity axis z direction, we have

$$E_{\rm ph} = \frac{\hbar c}{n} \sqrt{k_z^2 + k_{\parallel}^2} \approx \frac{\hbar c}{n} k_z + \frac{\hbar c}{2nk_z} k_{\parallel}^2, \tag{A1}$$

where we assumed  $k_z \gg k_{\parallel}$  to simplify the dispersion in the quadratic form in terms of the parallel momentum. Remembering that for a cavity length of L,  $k_z = \pi/L$  for the lowest mode, it becomes clear that for thin cavities with well-separated longitudinal mode manifolds, this is a valid assumption.

Based on Eq. (A1), we can define the following quantities, i.e., the longitudinal mode frequency  $\omega_c$  and the effective photon mass  $m_{\rm ph}$ , as

$$E_{\rm ph} = \hbar \omega_c + \frac{\hbar^2}{2m_{\rm ph}} k_{\parallel}^2, \quad \omega_c = \frac{c\pi}{nL}, \quad m_{\rm ph} = \frac{n\pi\hbar}{cL}.$$
 (A2)

With these, we can write the cavity Hamiltonian in terms of the field operators as

$$\hat{H}_{\text{cav}} = \int d\mathbf{r} \, \mathcal{E}^{\dagger}(\mathbf{r}) \Biggl( \hbar \omega_c + \frac{\hbar^2}{2m_{\text{ph}}} \nabla^2 \Biggr) \mathcal{E}(\mathbf{r}), \quad (A3)$$

where we used  $\nabla^2$  to describe the kinetic energy of the photons, i.e., energy of free photons propagating in the transverse direction, and dropped the subscript index as the dynamics are merely restricted to in-plane coordinates.

In the Heisenberg picture of evolving fields, one can derive the equations of motion (EoM) for the exciton- and cavity-field operators, which in general leads to an infinite hierarchy of the moments due to the correlation between excitons and photons. Since V is typically large at short distances [cf. Fig. 1(b)], the coupled field-exciton dynamics cannot be solved perturbatively. Instead, we seek a solution for small driving fields, corresponding to a cluster expansion in the exciton correlations. Since the leading-order nonlinearity is determined by terms up to pair correlations, the hierarchy can be truncated at this order. To first-order approximation, the correlations between the cavity photons and excitons can be ignored, expressing

$$\langle \hat{\mathcal{E}}^{\dagger}(\mathbf{r})\hat{X}(\mathbf{r})\rangle \approx \mathcal{E}(\mathbf{r})\langle \hat{X}(\mathbf{r})\rangle,$$
 (A4)

where we further assumed a weak exciton-cavity coupling, i.e., a negligible correlation, which means the cavity field is a coherent state.

Considering steady-state expectation values, a closed algebraic system of equations is obtained that can be solved in an expansion in the drive. To simplify the equations, we also assumed that the excitons are immobile compared to the much lighter photons, and hence they have no kinetic energy and the cavity dispersion is quadratic in the transverse momentum. As mentioned before, in the presence of many photons in the cavity field, quantum fluctuations can be ignored. However, truncating the cluster expansion at third order is only permissible at low exciton densities. Therefore, the generalized GPE in Eq. (1) of the main text is only valid within a certain range of cavity-field intensities.

Furthermore, from Eq. (3), one can define an important length scale, known as the blockade radius,

$$r_b = \left| \frac{C_6}{\Gamma_{\rm ex}} \right|^{\frac{1}{6}}.\tag{A5}$$

$$i\partial_t \begin{pmatrix} \delta E(\mathbf{k},t) \\ \delta E^*(-\mathbf{k},t) \end{pmatrix} = \begin{pmatrix} \frac{\mathbf{k}^2}{2} + 2\pi |E_0|^2 \tilde{W}(\mathbf{k}) & 2\pi E_0^2 \tilde{W}(\mathbf{k}) \\ -2\pi E_0^{*2} \tilde{W}^*(-\mathbf{k}) & -\frac{\mathbf{k}^2}{2} - 2\pi |E_0|^2 \tilde{W}^*(-\mathbf{k}) \end{pmatrix} \begin{pmatrix} \delta E(\mathbf{k},t) \\ \delta E^*(-\mathbf{k},t) \end{pmatrix},$$

where  $\delta E(\mathbf{k},t) = \mathcal{F}_{\mathbf{r}}[\delta \epsilon(\mathbf{r},t)] = \frac{1}{2\pi} \int d\mathbf{r} \delta \epsilon(\mathbf{r},t) e^{-i\mathbf{k}\cdot\mathbf{r}}$  and  $\tilde{W}(\mathbf{k}) = \mathcal{F}_{\mathbf{r}}[W(\mathbf{r}, t)]$ . Here,  $W(\mathbf{r})$  is real, which simplifies the dispersion as

$$\omega_{\pm}(k) = \pm \sqrt{\frac{k^2}{2} \left[ \frac{k^2}{2} + 4\pi |E_0|^2 \tilde{W}(k) \right]}.$$
 (B4)

Equation (B4) describes the energy-momentum relationship of the system around the stationary homogeneous or flat solution  $E_0$ . When the roton minimum softens, the spectrum acquires a positive imaginary part, consequently leading to instability and pattern formation.

While for distances below the blockade radius, the large van der Waals interaction re-normalizes the ensemble energy and hence saturates the interaction, at distances longer than  $r_b$ , the interaction asymptotically approaches the van der Waals potential dropping as  $r^6$ . As shown in Fig. 1(b), the photon-photon interaction is complex in general, having both dispersive and dissipative parts.

#### APPENDIX B: CLOSED-SYSTEM DYNAMICS

To investigate the effect of the nonlocal interactions, we start with the closed system with closed dynamics, i.e.,  $\kappa = \gamma = \eta = 0$ , satisfying the following GPE:

$$i\partial_t \mathcal{E} = \left[ -\frac{\hbar}{2m_{\rm ph}} \nabla^2 + i\chi^{(1)} + \int d\mathbf{r}' W(\mathbf{r} - \mathbf{r}') |\mathcal{E}(\mathbf{r}')|^2 \right] \mathcal{E}(\mathbf{r}).$$
(B1)

Note that this generalized GPE closely resembles the GPE describing the behavior of the condensate wave function in dipolar gases [8], implying similar behavior in both cases, including the emergence of the density patterns.

With the choice of scaling for the length and time as in Eq. (6) of the main text, the prefactor of the kinetic energy can be simplified to  $\hbar/m_{\rm ph} \to 1$ . From Eq. (B1), we find that the uniform solution  $\mathcal{E}(\mathbf{r},t) = E_0 e^{-i\mu_0 t}$  satisfies

$$\mu_0 E_0 = \left[ i\chi^{(1)} + 2\pi \tilde{W}(0) |E_0|^2 \right] E_0,$$
 (B2)

where  $2\pi \tilde{W}(0) = \int d\mathbf{r} W(\mathbf{r})$  is the average nonlinear susceptibility, i.e., an effective Kerr-type nonlinearity, and  $\mu_0$  is the chemical potential.

To study the dynamical stability, we consider a perturbation  $\delta \epsilon(\mathbf{r}, t)$  to the steady-state solution. After a Fourier transform, we can simplify the equations of motion for  $\delta E(\mathbf{k},t)$  as

$$\frac{2\pi E_0^2 \tilde{W}(\mathbf{k})}{-\frac{\mathbf{k}^2}{2} - 2\pi |E_0|^2 \tilde{W}^*(-\mathbf{k})} \begin{pmatrix} \delta E(\mathbf{k}, t) \\ \delta E^*(-\mathbf{k}, t) \end{pmatrix}, \tag{B3}$$

Figure 5 shows the dispersion of the closed system for  $|E_0|^2 = 10, 20, 30$  and for  $C_6 = -1, \Delta = -1$  (and hence  $r_b =$ 1). The real part depicted in Fig. 5(a) shows the roton minimum and softening for small values of k within (4.5, 6.5), where the dispersion vanishes and is accompanied by imaginary values shown in Fig. 5(b) corresponding to decaying and growing fluctuations, and hence the dynamical instability. For larger values of k, the dispersion is quadratic as for a free particle. The roton minimum and the associated instability can be a precursor of the supersolid phase.

To study the implications of the dynamic (in)stability of the polariton cloud, we investigate the time evolution of the system described by Eq. (B1). Figures 5(c) and 5(d) show the snapshots of the cavity field for  $|E_0|^2 = 10$  and  $|E_0|^2 = 30$ , respectively, using the slit-step Fourier method. In Fig. 5(d) and at t = 0, the field starts from a uniform solution with perturbed Gaussian noise, and as time evolves, patterns form due to the dynamical instability.

<sup>&</sup>lt;sup>1</sup>Here we use a symmetric Fourier transform, and hence  $\mathcal{F}[f(r) \otimes$ g(r)] =  $2\pi \tilde{F}(k)\tilde{G}(k)$ .

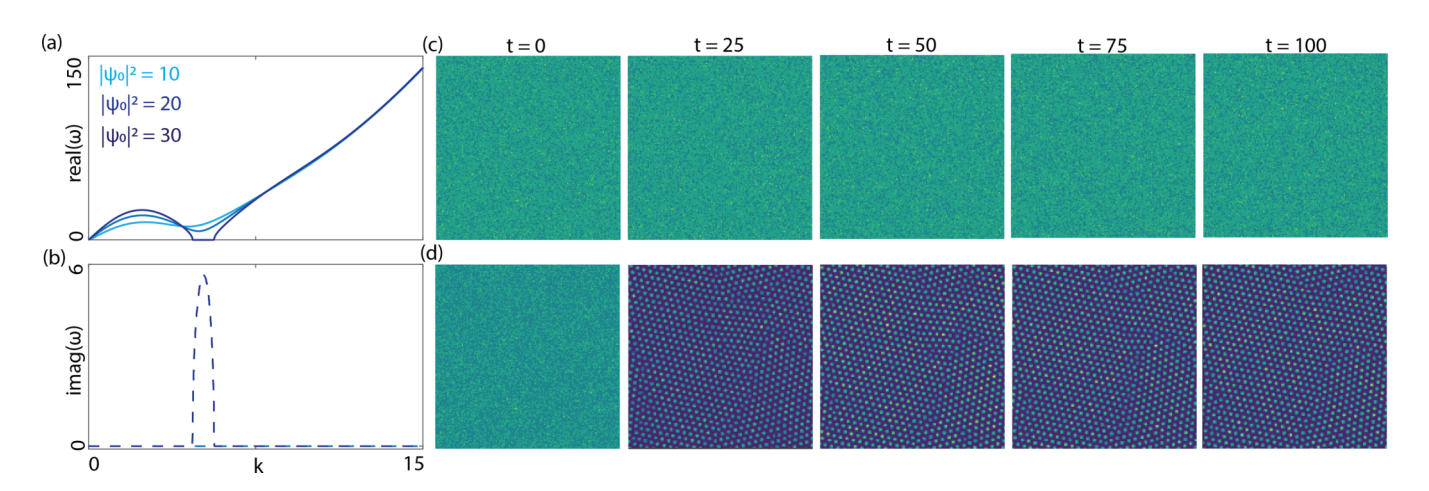


FIG. 5. Closed system. (a) Real and (b) imaginary part of the Bogoliubov dispersion for a closed system with no loss ( $\gamma = \kappa = \eta = 0$ ), when  $|E_0|^2 = 10$ , 20, 30 and g = 1,  $C_6 = -1$ ,  $\Delta = -1$ . Time evolution of the nonlocal GPE of the noisy flat-top solution within t = (0,100) for (c)  $|E_0|^2 = 10$  and (d)  $|E_0|^2 = 30$ .

# APPENDIX C: COMPARISONS WITH CONTACT INTERACTION

As discussed in the main text, for flat-top solutions in the steady state, the effect of long-range potential W(R) can be replaced with a contact interaction as  $2\pi \tilde{W}(0)$ . While this leads to similar steady-state behavior, in which the photon

density vs the pump rate is the same, the stability of the two types of interactions is different. Figures 6(a) and 6(b) shows the stable (solid line) and unstable (dashed line) solutions for contact and long-range interaction, respectively.

For the contact interactions, the Bogoliubov dispersion will be given as follows:

$$\omega_{\pm}(k) = i \left[ 4\pi |E_0|^2 \tilde{W}_I(0) + \chi_R^{(1)} - \frac{\kappa}{2} \right] \pm \sqrt{\left[ \frac{k^2}{2} + 4\pi |E_0|^2 \tilde{W}_R(0) - \chi_I^{(1)} - \Delta_c \right]^2 - 4\pi^2 |E_0|^4 \left[ \tilde{W}_R^2(0) + \tilde{W}_I^2(0) \right]}.$$
 (C1)

Figures 6(c) and 6(d) show the Bogoliubov spectrum of the contact and long-range interaction at  $E_0 = 16$ , respectively, where MI can be obtained in both cases.

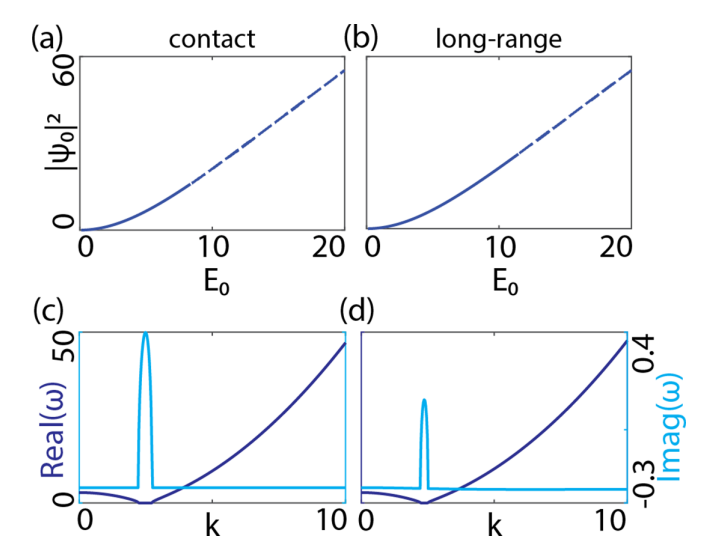


FIG. 6. Comparison between contact and long-range interactions. Steady-state vs coherent pump rate for (a) contact and (b) long-range interactions.

While the instability range and the gain values are different, the spectra are overall similar. However, as demonstrated in the main text, the pattern formation dynamics from the unstable homogeneous state is fundamentally different for short- and long-range interactions.

# APPENDIX D: OPEN SYSTEM WITH INCOHERENT DRIVE

For a spatially uniform incoherent pump, i.e.,  $P(\mathbf{r}) = P_0$ , we use the flat-top ansatz with the condensation frequency  $\omega_0$  as  $\mathcal{E}(\mathbf{r},t) = E_0 e^{-i\omega_0 t}$ , where

$$|E_0|^2 = \frac{1}{4\bar{W}_I} [\mathcal{B} \pm \sqrt{\mathcal{B}^2 - 8\bar{W}_I(P_0 - P_{\text{th}})}],$$
 (D1)

$$\omega_0 = \omega_c - \chi_I^{(1)} + \bar{W}_R |E_0|^2.$$
 (D2)

The threshold pumping power  $P_{th}$  and  $\mathcal{B}$  are defined as

$$P_{\rm th} = \frac{\gamma_R}{R} \left( \kappa - 2\chi_{\rm R}^{(1)} \right) \tag{D3}$$

and

$$\mathcal{B} = \frac{R}{\gamma_R} P_{\text{th}} - \frac{2\gamma_R}{R} \bar{W}_I. \tag{D4}$$

The stability of the flat-top solution can be determined via the following Bogoliubov matrix:<sup>2</sup>

$$\begin{pmatrix} \frac{\mathbf{k}^2}{2} + 2\pi E_0^2 \tilde{W}(\mathbf{k}) - i\Gamma/2 & 2\pi E_0^2 \tilde{W}(\mathbf{k}) - i\Gamma/2 \\ -2\pi E_0^2 \tilde{W}^*(\mathbf{k}) - i\Gamma/2 & -\frac{\mathbf{k}^2}{2} - 2\pi E_0^2 \tilde{W}^*(\mathbf{k}) - i\Gamma/2 \end{pmatrix},$$
(D5)

where we defined the small-signal pumping rate  $\Gamma$  as

$$\Gamma = \frac{R^2 P_0}{\left(\gamma_R + R\psi_0^2\right)^2} E_0^2.$$
 (D6)

#### APPENDIX E: EXPERIMENTAL CONSIDERATIONS

Observing excited Rydberg excitons presents a challenge, primarily due to most materials' typically small Rydberg constant. However,  $Cu_2O$  stands out as a rare exception with a significantly larger Rydberg constant, showcasing Rydberg states characterized by record principal quantum numbers, reaching n=30. In these highly excited states, excitons exhibit enhanced sensitivity to external fields, and their mutual interactions can be magnified by more than 10 orders of magnitude compared to the ground state.

Furthermore, the observed linewidths for Rydberg excitons up to n = 25 suggest lifetimes of 200–400 ps, which

is approximately an order of magnitude greater than excitons in GaAs quantum wells. The prolonged coherence times, coupled with the robust interactions in Rydberg states, hold tremendous potential for a diverse range of applications. The renewed interest in  $Cu_2O$  excitons has spurred numerous studies, detailed in recent review articles [26].

The recent experimental demonstration of Rydberg exciton polaritons from a  $\text{Cu}_2\text{O}$  layer surrounded by distributed Bragg reflector indicates that the realization of these quasiparticles is indeed feasible in a cavity with the moderate quality factor of  $Q \approx 2300$  [29]. With a vacuum Rabi cooling of  $g \approx 200$  GHz, hybridization of the first few Rydberg states up to n=6 has been demonstrated.

For cuprous oxide, the van der Waals (vdW) interaction coefficient and the decay rate vary with the principal quantum number (n) as [25]

$$c_6(n) \approx 10^{-2} n^{11} \,(\text{Hz um}^6),$$
 (E1)

$$\gamma_n \approx \frac{3.8}{n^3} \, (\text{THz}).$$
 (E2)

The required parameters in the main text can be obtained in a cavity with  $L\approx 300$  nm where a resonance at  $\lambda_c=575$  nm can be supported, and the requirement can be met for a cavity with  $\mathcal{F}\approx 20$ , with an active layer of Cu<sub>2</sub>O at  $n\sim 10$  and cooperativity of  $C\approx 3$ .

- [1] A. R. Liddle and D. H. Lyth, *Cosmological Inflation* and *Large-Scale Structure* (Cambridge University Press, Cambridge, 2000).
- [2] A. J. Koch and H. Meinhardt, Biological pattern formation: From basic mechanisms to complex structures, Rev. Mod. Phys. 66, 1481 (1994).
- [3] O. G. Mouritsen, Pattern formation in condensed matter, Intl. J. Mod. Phys. B **04**, 1925 (1990).
- [4] N. Henkel, R. Nath, and T. Pohl, Three-dimensional roton excitations and supersolid formation in Rydberg-excited Bose-Einstein condensates, Phys. Rev. Lett. 104, 195302 (2010).
- [5] F. Cinti, P. Jain, M. Boninsegni, A. Micheli, P. Zoller, and G. Pupillo, Supersolid droplet crystal in a dipole-blockaded gas, Phys. Rev. Lett. 105, 135301 (2010).
- [6] N. Henkel, F. Cinti, P. Jain, G. Pupillo, and T. Pohl, Supersolid vortex crystals in Rydberg-dressed Bose-Einstein condensates, Phys. Rev. Lett. 108, 265301 (2012).
- [7] V. Heinonen, K. J. Burns, and J. Dunkel, Quantum hydrodynamics for supersolid crystals and quasicrystals, Phys. Rev. A 99, 063621 (2019).
- [8] J. Hertkorn, J.-N. Schmidt, M. Guo, F. Böttcher, K. S. H. Ng, S. D. Graham, P. Uerlings, T. Langen, M. Zwierlein, and T. Pfau, Pattern formation in quantum ferrofluids: From supersolids to superglasses, Phys. Rev. Res. 3, 033125 (2021).

- [9] Y.-C. Zhang, T. Pohl, and F. Maucher, Phases of supersolids in confined dipolar Bose-Einstein condensates, Phys. Rev. A 104, 013310 (2021).
- [10] S. Ostermann, V. Walther, and S. F. Yelin, Superglass formation in an atomic BEC with competing long-range interactions, Phys. Rev. Res. 4, 023074 (2022).
- [11] L. Chomaz, I. Ferrier-Barbut, F. Ferlaino, B. Laburthe-Tolra, B. L. Lev, and T. Pfau, Dipolar physics: A review of experiments with magnetic quantum gases, Rep. Prog. Phys. 86, 026401 (2023).
- [12] F. Cinti, T. Macrì, W. Lechner, G. Pupillo, and T. Pohl, Defectinduced supersolidity with soft-core bosons, Nat. Commun. 5, 3235 (2014).
- [13] J. P. Corson, R. M. Wilson, and J. L. Bohn, Stability spectroscopy of rotons in a dipolar Bose gas, Phys. Rev. A 87, 051605(R) (2013).
- [14] M. Tlidi, P. Mandel, and R. Lefever, Localized structures and localized patterns in optical bistability, Phys. Rev. Lett. 73, 640 (1994).
- [15] T. Ackemann, Y. A. Logvin, A. Heuer, and W. Lange, Transition between positive and negative hexagons in optical pattern formation, Phys. Rev. Lett. **75**, 3450 (1995).
- [16] F. T. Arecchi, S. Boccaletti, and P. Ramazza, Pattern formation and competition in nonlinear optics, Phys. Rep. **318**, 1 (1999).

<sup>&</sup>lt;sup>2</sup>Note that in the simplification, we implicitly assumed that  $\psi_0$  is real, which does not impose any limitation due to the U(1) symmetry of the generalized GPE.

- [17] Y.-C. Zhang, V. Walther, and T. Pohl, Self-bound droplet clusters in laser-driven Bose-Einstein condensates, Phys. Rev. A 103, 023308 (2021).
- [18] Y.-C. Zhang, V. Walther, and T. Pohl, Long-range interactions and symmetry breaking in quantum gases through optical feedback, Phys. Rev. Lett. 121, 073604 (2018).
- [19] H. Haken, Towards a quantum synergetics: Pattern formation in quantum systems far from thermal equilibrium, Phys. Scr. 32, 274 (1985).
- [20] V. Ardizzone, P. Lewandowski, M.-H. Luk, Y.-C. Tse, N.-H. Kwong, A. Lücke, M. Abbarchi, E. Baudin, E. Galopin, J. Bloch, A. Lemaitre, P.-T. Leung, P. Roussignol, R. Binder, J. Tignon, and S. Schumacher, Formation and control of Turing patterns in a coherent quantum fluid, Sci. Rep. 3, 3016 (2013).
- [21] M. F. Maghrebi, M. J. Gullans, P. Bienias, S. Choi, I. Martin, O. Firstenberg, M. D. Lukin, H. P. Büchler, and A. V. Gorshkov, Coulomb bound states of strongly interacting photons, Phys. Rev. Lett. 115, 123601 (2015).
- [22] I. Carusotto and C. Ciuti, Quantum fluids of light, Rev. Mod. Phys. 85, 299 (2013).
- [23] H.-X. Wang, A. Zhan, Y.-D. Xu, H.-Y. Chen, W.-L. You, A. Majumdar, and J.-H. Jiang, Quantum many-body simulation using monolayer exciton-polaritons in coupled-cavities, J. Phys.: Condens. Matter 29, 445703 (2017).
- [24] S. Ghosh and T. C. H. Liew, Quantum computing with exciton-polariton condensates, npj Quantum Inf. 6, 16 (2020)
- [25] T. Kazimierczuk, D. Fröhlich, S. Scheel, H. Stolz, and M. Bayer, Giant Rydberg excitons in the copper oxide  $Cu_2O$ , Nature (London) **514**, 343 (2014).
- [26] M. Aßmann and M. Bayer, Semiconductor Rydberg physics, Adv. Quantum Technol. 3, 1900134 (2020).
- [27] V. Walther, R. Johne, and T. Pohl, Giant optical nonlinearities from Rydberg excitons in semiconductor microcavities, Nat. Commun. 9, 1309 (2018).
- [28] J. Gu, V. Walther, L. Waldecker, D. Rhodes, A. Raja, J. C. Hone, T. F. Heinz, S. Kéna-Cohen, T. Pohl, and V. M. Menon, Enhanced nonlinear interaction of polaritons via excitonic Rydberg states in monolayer WSe<sub>2</sub>, Nat. Commun. 12, 2269 (2021).

- [29] K. Orfanakis, S. K. Rajendran, V. Walther, T. Volz, T. Pohl, and H. Ohadi, Rydberg exciton–polaritons in a Cu<sub>2</sub>O microcavity, Nat. Mater. 21, 767 (2022).
- [30] V. Walther, S. O. Krüger, S. Scheel, and T. Pohl, Interactions between Rydberg excitons in Cu<sub>2</sub>O, Phys. Rev. B **98**, 165201 (2018).
- [31] Note that in general, the spinor and the Bogoliubov matrix entries must have terms as  $\delta \Psi^*(-\mathbf{k},t)$  and  $\tilde{W}(-\mathbf{k})$ , i.e., the time-reversed transforms. However, since the functions are centrosymmetric, i.e.,  $f(\mathbf{r}) = f(-\mathbf{r})$ , the transforms are centrosymmetric as well and hence we do the simplification directly.
- [32] M. Wouters and I. Carusotto, Excitations in a nonequilibrium Bose-Einstein condensate of exciton polaritons, Phys. Rev. Lett. **99**, 140402 (2007).
- [33] K. G. Lagoudakis, M. Wouters, M. Richard, A. Baas, I. Carusotto, R. André, L. S. Dang, and B. Deveaud-Plédran, Quantized vortices in an exciton-polariton condensate, Nat. Phys. 4, 706 (2008).
- [34] L. Klaus, T. Bland, E. Poli, C. Politi, G. Lamporesi, E. Casotti, R. N. Bisset, M. J. Mark, and F. Ferlaino, Observation of vortices and vortex stripes in a dipolar condensate, Nat. Phys. 18, 1453 (2022).
- [35] J. P. Moroney and P. R. Eastham, Synchronization in disordered oscillator lattices: Nonequilibrium phase transition for driven-dissipative bosons, Phys. Rev. Res. 3, 043092 (2021).
- [36] X. Ma, U. Peschel, and O. A. Egorov, Incoherent control of topological charges in nonequilibrium polariton condensates, Phys. Rev. B 93, 035315 (2016).
- [37] T. Graß, P. Bienias, M. J. Gullans, R. Lundgren, J. Maciejko, and A. V. Gorshkov, Fractional quantum Hall phases of bosons with tunable interactions: From the Laughlin liquid to a fractional Wigner crystal, Phys. Rev. Lett. 121, 253403 (2018).
- [38] C. D. Parmee and J. Ruostekoski, Cooperative optical pattern formation in an ultrathin atomic layer, Opt. Express **31**, 42046 (2023).
- [39] K. Kwon, K. Mukherjee, S. J. Huh, K. Kim, S. I. Mistakidis, D. K. Maity, P. G. Kevrekidis, S. Majumder, P. Schmelcher, and J.-Y. Choi, Spontaneous formation of star-shaped surface patterns in a driven Bose-Einstein condensate, Phys. Rev. Lett. 127, 113001 (2021).